Journal of Power Sources 245 (2014) 171–174

Contents lists available at SciVerse ScienceDirect

Journal of Power Sources

journal homepage: www.elsevier.com/locate/jpowsour

Short communication

# Nickel catalysts for hydrogen evolution from $CsH_2PO_4$

Alexander B. Papandrew [a,*], Thomas A. Zawodzinski Jr. [a,b]

[a] Department of Chemical and Biomolecular Engineering, University of Tennessee, Knoxville, TN 37996, USA
[b] Materials Science and Technology Division, Oak Ridge National Laboratory, Oak Ridge, TN 37831, USA

## HIGHLIGHTS

- Electrochemical hydrogen pumps were fabricated with $CsH_2PO_4$ membranes.
- Ni-based electrodes evolve hydrogen at >200 mA $cm^{-2}$ at −0.2 V.
- Ni-based electrodes have a limited hydrogen oxidation activity.
- Hydrogen oxidation/evolution is reversible on Pt electrodes.

## ARTICLE INFO

*Article history:*
Received 23 March 2013
Received in revised form
11 June 2013
Accepted 25 June 2013
Available online 4 July 2013

*Keywords:*
Solid acids
Inorganic proton conductors
Hydrogen evolution
Non-precious catalysts

## ABSTRACT

Unsupported nickel was evaluated as an electrocatalyst material in an electrochemical hydrogen pump using the superprotonic solid acid $CsH_2PO_4$ as a proton exchange membrane. In humidified hydrogen at 250 °C, Ni-based electrodes display a stable proton reduction current of 207 mA $cm^{-2}$ at a −0.2 V cell potential. Electrodes utilizing carbon-supported Pt catalysts evolved hydrogen at 558 mA $cm^{-2}$ under identical conditions. Hydrogen evolution and oxidation are reversible on Pt, but hydrogen oxidation activity is virtually absent on Ni.



## 1. Introduction

The economical large-scale production of pure molecular hydrogen as an energy storage medium remains an open problem. Electrochemical routes to hydrogen fuel have expanded in recent years, given concerns regarding the availability of fossil fuels and the damaging environmental consequences of hydrocarbon oxidation. Common to each electrochemical hydrogen production route, be it liquid water electrolysis [1], steam electrolysis [2], photocatalytic electrolysis [3] or less-common methods such as the hybrid-sulfur (HyS) process [4], is the need to evolve hydrogen at a catalytically active electrode. The HER is also central to electrochemical hydrogen pumps [5,6], which produce pure hydrogen from multicomponent input streams derived from heterogeneous fuel reforming. Typical catalysts for the HER include the platinum-group metals (PGM) [7], an unfortunately rare and expensive class of materials that raise economic barriers to the adoption of the aforementioned technologies.

Almost uniformly, non-precious alternative HER catalysts are evaluated in aqueous alkaline or acid solutions in three-electrode electrochemical cells. A prerequisite for functional hydrogen production technologies is the eventual implementation of catalysts in bipolar stacks that can evolve hydrogen at a high rates via porous gas-diffusion electrodes. The properties of these devices are highly contingent on constraints imposed by the electrolyte, including catalyst stability, activity, and impurity tolerance.

An emerging electrolyte material that has potential for coupling to the vast array of available HER catalysts is the anhydrous inorganic proton conductor $CsH_2PO_4$ (CDP). CDP is distinguished by a polymorphic phase transition at 228 °C that results in a large increase in proton conductivity (from $8.5 \times 10^{-6}$ S $cm^{-1}$ at 223 °C to $2.5 \times 10^{-2}$ S $cm^{-1}$ at 250 °C). CDP is attractive for electrochemical hydrogen pumping due to the impurity tolerance of catalysts in its operational temperature range; $H_2$-air cells based on CDP electrolytes are capable of stable operation on reformate streams containing 20% CO [8].

* Corresponding author.
*E-mail addresses:* apapandrew@utk.edu (A.B. Papandrew), tzawodzi@utk.edu (T.A. Zawodzinski).

0378-7753/$ – see front matter © 2013 Elsevier B.V. All rights reserved.
http://dx.doi.org/10.1016/j.jpowsour.2013.06.141

In this communication, we report on our initial investigations of non-PGM catalysts for hydrogen evolution from superionic CDP. Nickel is well-known for HER activity in aqueous acid [9] systems, and has recently been the subject of renewed interest in the HER in alkaline systems [10]. Here, Ni is demonstrated as the first possible substitute for noble metals in a system based on solid acid electrolytes. Electrochemical hydrogen pumps were fabricated with either symmetric Pt-based gas diffusion electrodes or a Ni-based gas diffusion electrode and a conjugate Pt electrode and evaluated for electrochemical activity, reversibility, and stability.

## 2. Experimental methods

Coarse $CsH_2PO_4$ was synthesized by reaction of $Cs_2CO_3$ (Alfa Aesar, 99%) with orthophosphoric acid (Alfa Aesar, 85%) followed by precipitation in methanol and drying. Fine particulate CDP was derived by low-energy ball-milling the coarse CDP powder. Platinum supported on Vulcan XC-72R (60 wt%) was synthesized by vapor-phase decomposition of $Pt(acac)_2$ (Alfa Aesar, Pt 48% min) in a fixed bed at 210 °C in a $N_2$/water vapor atmosphere via a protocol identical to the procedure reported previously [11]. Unsupported nickel nanoparticles (Sigma–Aldrich, ≥99%, P/N 577995, lot MKBK8685V) were used as received. The structure of the Ni powder was characterized with monochromatic Cu K$\alpha$ x-ray diffraction (XRD) (Philips X'Pert, $\lambda = 0.1541874$ nm, 45 kV, 40 mA, 0.04° step, 2.0 s/step), scanning electron microscopy (SEM) (LEO 1525, 3 kV accelerating voltage) and BET nitrogen adsorption surface area analysis (Quantachrome Autosorb iQ).

Composite electrocatalyst powders were synthesized from these starting materials by dry-grinding components using an agate mortar and pestle. In the case of Pt-based electrocatalyst, fine CDP, 60 wt%Pt/C, and naphthalene (as a fugitive binder) were combined in a 3:1:1 ratio by weight, respectively. Similarly, Ni-based electrocatalysts were comprised of fine CDP, Ni, Vulcan XC-72 carbon, and naphthalene in a 3:3:0.6:1 ratio.

Membrane-electrode assemblies (MEAs) were fabricated by sequential, uniaxial pressing of active layers in a hardened steel die with a 0.75 in diameter (2.85 $cm^2$) at 125 MPa. Stainless steel mesh (grade 304) served as the current collector for each electrode. Expanded PTFE tape was used to seal the electrodes and restrict the active area of each electrode to approximately 1.35 $cm^2$. Each MEA had a CDP membrane thickness of approximately 60 μm. In the case of the Pt control MEA, both electrodes were comprised of 25 mg of the Pt-based electrocatalyst (resulting in a Pt loading of 1.05 $mg_{Pt}\ cm^{-2}$ per electrode). The experimental Ni MEA replaces one of these electrodes with 25 mg of the Ni-based electrocatalyst (3.5 $mg_{Ni}\ cm^{-2}$).

Electrochemical testing was conducted in stainless steel test rigs at temperatures from 230 to 250 °C. Both electrodes were supplied flows of 30 sccm of ultrahigh purity $H_2$ hydrated to a dew point of 75 °C (approximately 0.3 bar water partial pressure) to prevent the dehydration phase transformation of superprotonic CDP [8]. Polarization curves were recorded at 30 min intervals with a Bio-Logic VSP potentiostat by scanning the working electrode potential at 2 mV $s^{-1}$ from 0.2 V to −0.2 V. Potentiostatic electrochemical impedance spectroscopy (PEIS) spectra were also recorded at selected potentials in a frequency range from 200 kHz to 200 mHz with a single sine perturbation amplitude of 10 mV. Polarization curves free of the ohmic losses due to membrane resistance were derived by the subtraction of $iR_\Omega$, where $i$ is the current and $R_\Omega$ is the dc resistance of the cell as measured at OCV by PEIS. Cells were held at −0.2 V for each 30 min interval between electrochemical measurements, and an identical potential was used for long-term tests.

## 3. Results and discussion

Fig. 1 shows the XRD pattern obtained from the as-received Ni powder. The powder is primarily composed of the fcc phase, but also contains the hcp phase as well as NiO, the latter which we expect to be reduced in the presence of hydrogen. Analysis with the X'Pert Highscore Plus software [12] determined a phase composition of 79.4% fcc Ni, 12.8% NiO, and 7.7% hcp Ni. The inset of Fig. 1 shows an SEM micrograph of the powder, revealing something of a bimodal particle size distribution consisting of larger, 200–300 nm particles supporting smaller particles 10–20 nm in size. The BET surface area of the powder was 12.7 $m^2\ g^{-1}$.

Hydrogen evolution polarization curves for the Pt control MEA and the experimental Ni MEA at 250 °C are shown in Fig. 2. The left panel of Fig. 2a shows traces uncorrected for the electrolyte membrane resistance $R_\Omega$. The linear response of the Pt electrode suggests ohmic control. Curvature is observed in the Ni response at low overpotentials, a typical hallmark of rate controlled by catalytic activation. In Fig. 2b, the cell voltages of each MEA have been corrected for the electrolyte resistance and the electrode responses plotted in Tafel form using an absolute, logarithmic current scale. Here we clearly observe a symmetric HOR/HER response from the Pt control, but a highly asymmetric response from the experimental Ni MEA.

Discussions of the HOR/HER are aided by introduction of the Butler–Volmer equation

$$i = i_0\left[e^{\alpha_a F\eta/RT} - e^{-\alpha_c F\eta/RT}\right] \quad (1)$$

where $i_0$ is the exchange current, $\alpha_a$ and $\alpha_c$ are the anodic and cathodic transfer coefficients, respectively, $\eta$ is the overpotential, $R$ is the gas constant, and $T$ is the Kelvin temperature. In the case of a rate-limiting electron transfer step for the HOR/HER, Equation (1) is equivalent to

$$i = i_0\left[e^{\beta F\eta/RT} - e^{-(1-\beta)F\eta/RT}\right] \quad (2)$$

where the transfer coefficient have been replaced by the symmetry factor, $\beta$, which takes a value of 0.5 for a symmetric activation

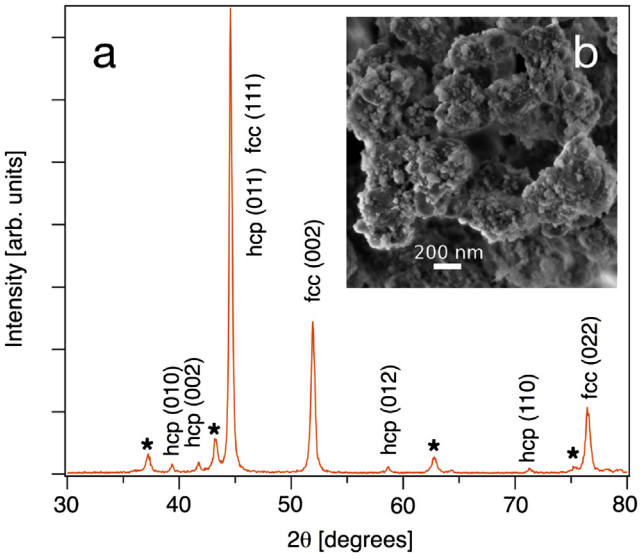


**Fig. 1.** (a) Cu Kα X-ray diffraction pattern from as-received Ni powder. Major peaks for the fcc and hcp structures are indexed; NiO peaks are marked with ★. (b) (inset) Scanning electron micrograph of as-received Ni powder acquired at 3 kV accelerating voltage.

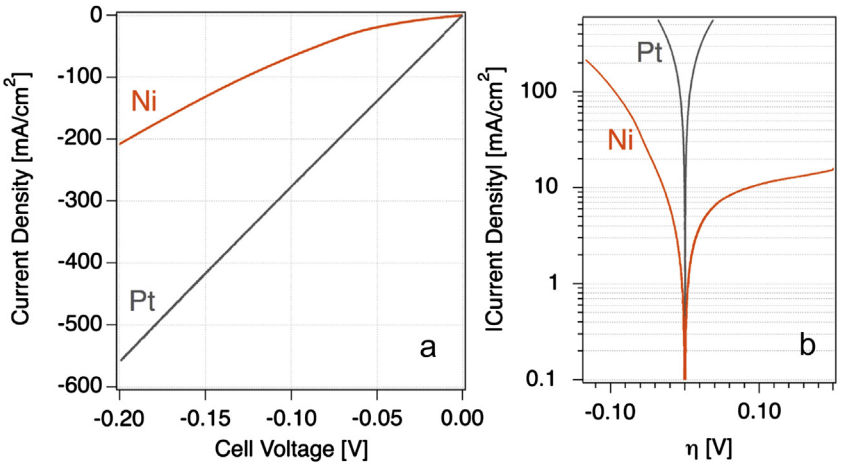


**Fig. 2.** (a) Hydrogen evolution polarization curve (uncorrected for $iR_\Omega$) for experimental Ni electrode and Pt control electrode and (b) $iR_\Omega$-corrected Tafel plots recorded at 250 °C in $H_2/H_2$ at 75 °C dew point.

barrier. Here we set the product of coverage-dependent prefactors ($\theta_j$) to be unity. Equation (2) was used to fit the $iR_\Omega$-free response of the Pt MEA across the investigated temperature range (230–250 °C), with $i_0$ and $\beta$ as free parameters. Values of $\beta$ of approximately 0.45 were obtained at all temperatures, and at 250 °C an exchange current density (normalized to electrode geometric area, 1.37 cm$^2$) of 656 mA $cm_{geo}^{-2}$ was found. Since determining the electrochemical surface area of electrodes based on solid acid electrolytes is still an open problem [13], we attempted to place a bound the active area of the Pt electrode using conventional aqueous electrochemistry. In $N_2$-saturated voltammetry measurements at room temperature in 0.1 M $HClO_4$, an electrochemical surface area for the 60%Pt/C catalyst of 45 m$^2$ $g_{pt}^{-1}$ was found based on an assumed H desorption charge of 210 μC $cm_{pt}^{-2}$. In the absence of a liquid or polymer electrolyte, we expect the ECSA of the actual CDP-based electrode to be much lower than this value. Nevertheless, using the obtained value of 45 m$^2$ $g_{pt}^{-1}$, we find a minimum exchange current density of 1.46 mA $cm_{pt}^{-2}$. Using a simple Arrhenius relationship for the temperature dependence of the exchange current, we plotted the logarithm of $i_0$ against $1/T$, finding an activation energy of 20.8 kJ mol$^{-1}$ for HOR/HER on Pt. This value is slightly lower than what is found for Pt/C in 0.1 M KOH (29.5 kJ mol$^{-1}$) [14], and in good agreement with results on Pt(111) surfaces in 0.05 M sulfuric acid (18 kJ mol$^{-1}$) [15] and Pt in phosphoric acid (16.7 kJ mol$^{-1}$) [16].

In the case of the experimental Ni electrode, it is clear that significant asymmetry in the rate of the HOR/HER is present, indicating a possibility of a mechanistic difference for the two reactions on Ni, even though they are symmetric on Pt. Based on the observed hydrogen oxidation current, The effective anodic transfer coefficient for hydrogen oxidation on Ni approaches 0. In the low-field approximation, Equation (1) can be expressed

$$i = i_0 \frac{\eta F}{RT} \tag{3}$$

and the polarization resistance for low $\eta$ is similarly defined as $\eta = iR_{ct}$ where $R_{ct}$ is the charge transfer resistance. Then by simple algebra we can derive the exchange current if $R_{ct}$ is known for low values of $\eta$. Here we have used EIS at OCV to find $R_{ct}$.

Nyquist plots for the experimental Ni MEA as a function of temperature are shown in Fig. 3. Though EIS probes both electrodes, the impedance due to the Pt electrode is very small (0.05 Ω cm$^2$, see Fig. 4) compared with the $R_{ct}$ for the Ni electrode,

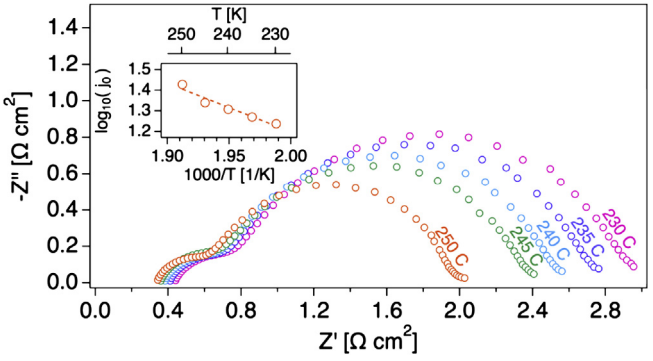


**Fig. 3.** Nyquist plots of PEIS (10 mV perturbation, 200 kHz to 200 mHz) spectra for the experimental Ni MEA at OCV and selected temperatures recorded in $H_2/H_2$ at 75 °C dew point. Inset shows the Arrhenius plot used to determine exchange current.

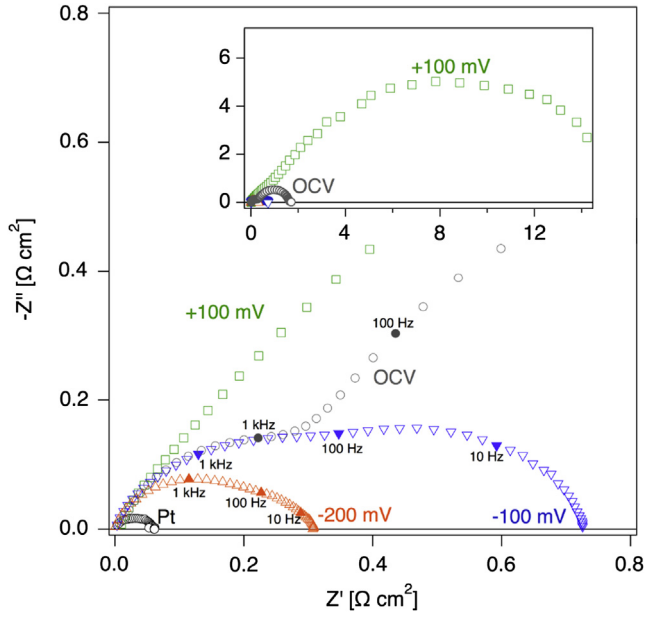


**Fig. 4.** $iR_\Omega$-free Nyquist plots of PEIS (10 mV perturbation, 200 kHz to 200 mHz) spectra for the experimental Ni MEA at selected polarizations and the Pt control MEA at OCV, recorded at 250 °C in $H_2/H_2$ at 75 °C dew point. Inset shows the full impedance range.

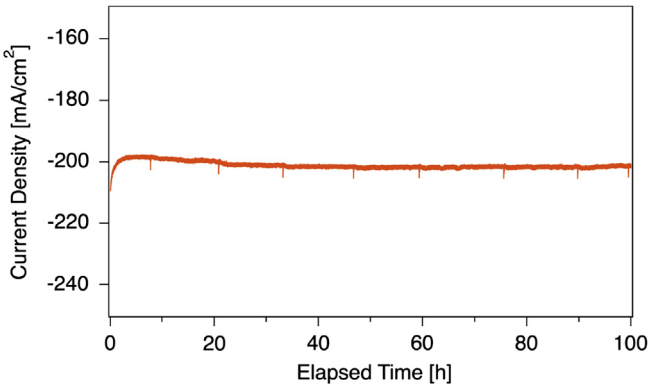


**Fig. 5.** Long term hydrogen evolution current of the experimental Ni MEA at 250 °C in $H_2/H_2$ at 75 °C dew point and −0.2 V working electrode potential.

and here we neglect it. In addition to the widening of the impedance arc with decreasing temperature, we note also the increased ohmic resistance associated with decreasing electrolyte conductivity. At 250 °C, we find a geometric exchange current density for the HER on Ni of 26.6 mA $cm^{-2}_{geo}$. Though determining ECSA for Ni catalysts in solid acid environments is even more difficult than for Pt, we bound our result by using the BET surface area of the Ni particles, 12.7 $m^2\ g^{-1}$. Normalizing the obtained value to the total surface area of the Ni in the electrode provides a lower bound on the exchange current density of 0.06 mA $cm^{-2}_{Ni}$. We find the ratio of this value to what was determined for Pt to be within a factor of 5 of tabulated values obtained in $H_2SO_4$ [9]. Again using the Arrhenius relation, we find an activation energy for the HER on Ni to be 45 kJ $mol^{-1}$.

The extreme asymmetry of the HOR/HER on Ni in the solid acid system is not well understood. Fig. 4 shows the variation of the impedance response of the Ni electrode with polarization. Under cathodic polarization the impedance response shrinks, indicative of a Faradaic process. However, anodic polarization causes a large increase in the electrode impedance, especially at lower frequencies. This may be evidence of a mass transport limitation or the blocking of binding sites for the dissociative adsorption of hydrogen on the catalyst surface. In alkaline media, for example, the potential-dependent presence of hydroxyl adsorbates on Ni-decorated Pt [17] enhances the rate of the HOR. However, in the present case, if the Ni surface is saturated with species that act as poisons rather than reaction intermediates, the HOR is unable to proceed. More detailed mechanistic studies are required to unravel the root cause of the reaction asymmetry on Ni.

Hydrogen evolution from the Ni electrode is stable for 100 h under steady-state conditions at 250 °C. Fig. 5 shows the result of this experiment. There is a slight initial decrease in the evolution current, possibly due to microstructural changes in the electrode, a phenomenon previously identified in electrodes for $H_2$-air cells based on CDP. The periodic fluctuations in the steady-state current density shown in Fig. 4 are of a magnitude of approximately 3 mA $cm^{-2}$ and return to the baseline level in approximately 4 min. It is likely that these excursions are related to small changes in hydrogen partial pressure due to water condensation and vaporization in the test fixture hardware.

For the fixed, identical flow rates and relatively thick membranes employed in this study, the hydrogen separation efficiency (the fraction of the inlet hydrogen that is electrochemically pumped across the membrane) is approximately 28% for the Pt symmetric cell, and 10% for the experimental Ni cell at respective −0.2 V overpotentials. Energy efficiencies are similar, 24% for Pt and 9% for Ni. We expect that these values can be improved by more aggressive flow stoichiometric ratios and thinner membranes in future work.

## 4. Conclusions

We have demonstrated that Ni is an effective catalyst for hydrogen evolution from superprotonic $CsH_2PO_4$ at temperatures above 230 °C. Though not nearly as active as Pt, Ni is considerably less expensive and shows promise for implementation in hydrogen separation and steam electrolysis applications using solid acid membranes. We expect that the performance of Ni-based HER electrodes can be further improved by the optimization of the electrode microstructure and dispersion of the catalyst.

## Acknowledgments

The authors gratefully acknowledge support from the Office of Naval Research (Award N000141210887). A.B.P Thanks Gabriel Goenaga and Samantha Hawks for electrochemical surface area measurements.

## References

[1] K. Zeng, D. Zhang, Prog. Energy Combust. Sci. 36 (2010) 307–326.
[2] P.A. Lessing, J. Mater. Sci. 42 (2007) 3477–3487.
[3] N.S. Lewis, D.G. Nocera, Proc. Natl. Acad. Sci. 103 (2006) 15729–15735.
[4] J. OBrien, J. Hinkley, S. Donne, S.-E. Lindquist, J. Electrochem. Soc. 55 (2010) 573–591.
[5] H. Iwahara, Y. Asakura, K. Katahira, M. Tanaka, Solid State Ionics 168 (2004) 299–310.
[6] K.A. Perry, G.A. Eisman, B.C. Benicewicz, J. Power Sources 177 (2008) 478–484.
[7] S. Grigoriev, P. Millet, V. Fateev, J. Power Sources 177 (2008) 281–285.
[8] C.R.I. Chisholm, D.A. Boysen, A.B. Papandrew, S.K. Zecevic, S. Cha, K.A. Sasaki, A. Varga, K.P. Giapis, S.M. Haile, Electrochem. Soc. Interface 18 (2009) 53–59.
[9] S. Trasatti, J. Electroanal. Chem. Interfacial Electrochem. 39 (1972) 163–184.
[10] R. Subbaraman, D. Tripkovic, D. Strmcnik, K.-C. Chang, M. Uchimura, A.P. Paulikas, V. Stamenkovic, N.M. Markovic, Science 334 (2011) 1256–1260. (New York, N.Y.).
[11] A.B. Papandrew, C.R.I. Chisholm, R.A. Elgammal, M.M. Özer, S.K. Zecevic, Chem. Mater. 23 (2011) 1659–1667.
[12] Philips Analytical B.V., Philips X'Pert Highscore Plus (1999).
[13] A.B. Papandrew, C.R.I. Chisholm, S.K. Zecevic, G.M. Veith, T.A. Zawodzinski, J. Electrochem. Soc. 160 (2013) F175–F182.
[14] W. Sheng, H.A. Gasteiger, Y. Shao-Horn, J. Electrochem. Soc. 157 (2010) B1529.
[15] N.M. Marković, B.N. Grgur, P.N. Ross, J. Phys. Chem. B 101 (1997) 5405–5413.
[16] W. Vogel, L. Lundquist, P. Ross, P. Stonehart, Electrochim. Acta 20 (1975) 79–93.
[17] D. Strmcnik, M. Uchimura, C. Wang, R. Subbaraman, N. Danilovic, D. van der Vliet, A.P. Paulikas, V.R. Stamenkovic, N.M. Markovic, Nat. Chem. 5 (2013) 300–306.